energy&fuels

pubs.acs.org/EF Article

Microfluidic Investigation of Salinity-Induced Oil Recovery in Porous Media during Chemical Flooding

Sung wan Park, Jonghyun Lee, Hongkyu Yoon, and Sangwoo Shin*

Cite This: *Energy Fuels* 2021, 35, 4885−4892 Read Online

ACCESS | Metrics & More | Article Recommendations | Supporting Information

ABSTRACT: High and low salinity water flooding are common oil recovery processes performed in the oil fields for extracting crude oil from the reservoir. These processes are often performed sequentially, naturally establishing non-uniform salinity in the porous subsurface. In this article, we investigate oil transport in porous media induced by salinity change upon flooding with high and low salinity water. As we observe a large number of impervious dead-ends from three-dimensional imaging of the actual reservoir, we identify that these areas play an important role in oil recovery where the oil transport is governed by the salinity change rather than hydrodynamics. The salinity gradients induced upon high salinity water flooding provide pathways to enhance the transport of oil drops trapped in the dead-end regions *via* non-equilibrium effects. However, above a critical salinity, we observe a rapid aggregation of drops that lead to the complete blockage of the pore space, thereby inhibiting oil recovery. We also find that, at an intermediate salinity where the drop aggregation is modest, the aggregation rather promotes the oil recovery. Our observations suggest that there exist optimal salinity conditions for maximizing oil recovery during chemical flooding.

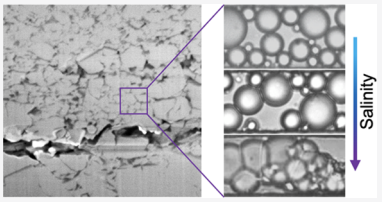

1. INTRODUCTION

Crude oil is the largest non-renewable source of energy that still has the highest demand worldwide as of 2019.[1] In general, the oil is extracted from the underground reservoir by first drilling a well directly down to the subsurface, thereby recovering approximately 10% of the initial oil (primary oil recovery).[2] Often, another well is drilled adjacent to the existing well, which serves as an injection well to flood the reservoir with inexpensive water (commonly seawater) so as to further extract the remaining oil (secondary oil recovery);[3] the secondary oil recovery can recover up to approximately 20−40% of the crude oil that was held in the original reservoir.[2]

With the added economic expense of drilling a secondary well, further extractions are typically done through tertiary oil recovery, or the enhanced oil recovery process. Enhanced oil recovery, which has the potential to remove an additional 30−60% of oil from the original reservoir, involves the injection of chemically engineered fluids such as polymers/surfactants/alkali solutions and low salinity water to improve the sweep efficiency and pore-scale displacement.[4]

Low salinity water flooding is a relatively recently developed chemical flooding that uses water with salinity ranging from 1000 to 2000 ppm to enhance oil recovery.[5,6] The benefit of using low salinity water over other chemicals is the simplicity, environmental friendliness, and low cost of operation. While many lab and field studies have proven the improved recovery in low salinity water flooding for decades, it still lacks understanding and general consensus on the key mechanism.[2,6−9] Most of the suggested possible mechanisms responsible for enhanced efficiency in low salinity water flooding are related to static interfacial phenomena such as the wettability and capillarity effects.[6−10] In contrast, mechanisms attributed to non-equilibrium transport phenomena of components of saline solution and their interactions with oil phase are rather rarely discussed in the literature and thus are not well understood.

In secondary and tertiary recovery with saline water, i.e., seawater and low salinity water flooding, respectively, displacement fluids are mixed with preceding solutions, commonly multiple times through which a non-uniform salinity is established within the tortuous reservoir spatially and temporally.[11] In addition, Saffman−Taylor instability (viscous fingering) further promotes such non-uniform salinity.[12] Recently in the colloids community, solute gradients have been identified as a pathway to accelerate the transport of colloids including oil drops in dead-end pores *via* non-equilibrium physicochemical processes, particularly by diffusiophoresis, suggesting its possible relevance in salinity-mediated water flooding.[13−20]

In this article, we investigate the oil transport in porous media induced by salinity change upon flooding. We show that the oil transport within the dead-ends can have a significant impact on the overall oil recovery efficiency depending on the water salinity and its local gradients. As it is unfeasible to

Received: December 22, 2020
Revised: February 16, 2021
Published: March 2, 2021

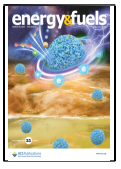

https://dx.doi.org/10.1021/acs.energyfuels.0c04320
Energy Fuels 2021, 35, 4885−4892

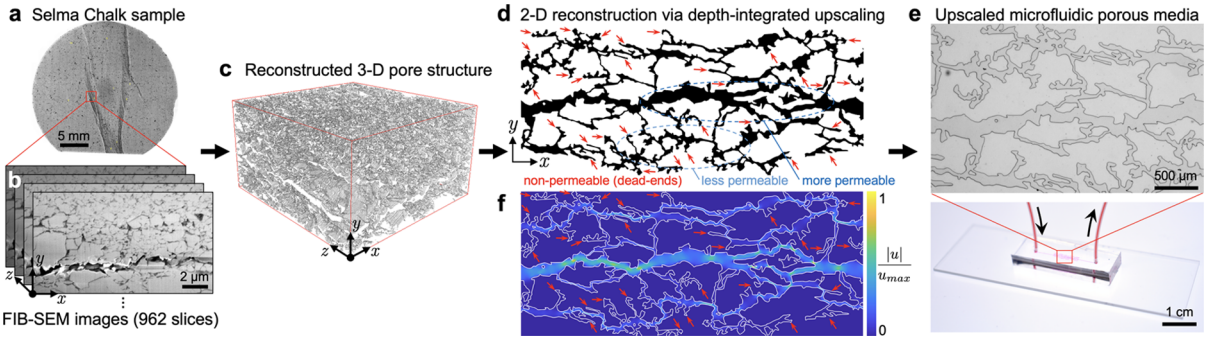

Figure 1. Fabrication of a two-dimensional model microfluidic reservoir from the three-dimensional morphology of an actual subsurface. (a) Thin section image of a Selma Chalk sample. The white region represents microfractures, and the dark gray region represents clay seams. (b) Stack of focused ion beam scanning electron microscopy (FIB-SEM) images at a 15.6 nm resolution in the slicing (z-) direction. Serial sectioning of 962 slices was performed. (c) The 2-D SEM images were interpolated and assembled into a 3-D pore structure. (d) The 3-D image was further processed to obtain a depth-integrated 2-D image with similar porosity and connectivity for microfluidic design. White is the solid phase, and black is the pore phase. (e) Fabricated microfluidic porous media using the 2-D reconstructed geometry in (d) as the photolithography mask. (f) Lattice Boltzmann simulation of the flow field in the same 2-D porous media shown in (e). The color legend indicates velocity magnitude normalized by the maximum flow velocity. The red arrows in (d) and (f) indicate dead-end regions, which exhibit zero flow velocity.

directly visualize and characterize the underground reservoir in real-time during oil recovery operations, it is important to perform lab-scale visualization of the oil displacement in the subsurface, which will allow a deeper understanding of the transport processes so as to achieve better recovery efficacy.[21,22] In this regard, the use of microfluidic devices offers easy real-time visualization that models the oil recovery in porous reservoirs due to the channel materials typically being transparent (*e.g.*, glass, polydimethylsiloxane (PDMS), poly(methyl methacrylate) (PMMA), and UV-curable epoxy).[23] Here, we use actual reservoir data to closely mimic the morphology of the porous subsurface with transparent microfluidic devices. Rather than investigating the well-studied wetting behavior induced by the salinity effects, we focus on the transport aspect of oil dynamics during saline water flooding, particularly at high oil volume fraction, which will provide a unique understanding of the water flooding *via* a non-equilibrium transport process (i.e., diffusiophoresis) that has been largely overlooked in the petroleum literature.

2. MATERIALS AND METHODS

2.1. Fabrication of Model Microfluidic Reservoirs. We created model microfluidic porous media from a full three-dimensional (3-D) morphology of an actual subsurface reservoir (Figure 1). A 1 inch diameter plug of Selma group chalk (Navarro Formation) was extracted from the core (1891.1 m belowground surface) near Escatawpa, Mississippi, USA, where the porosity and permeability of the core plug were measured as 12.5−16.7% and 0.012−0.108 mD, respectively (Figure 1a). Core sampling was performed during the National Energy Technology Laboratory's Southeast Regional Carbon Sequestration Partnership Phase II.[24] From this sample, serial sectioning and imaging was performed *via* focused ion beam scanning electron microscopy (FIB-SEM; FEI Helios 600 Nanolab DualBeam) of 962 slices, equivalent to approximately 15 μm in the slicing (z-) direction, and 16 μm × 10 μm per image (Figure 1b). Subsequently, the stack of SEM images was binarized and then assembled into a 3-D pore structure (Figure 1c).[25] In this study, the 3-D structure was further processed with depth averaging and iterative thresholding to obtain a depth-integrated two-dimensional (2-D) image with similar porosity and connectivity (Figure 1d). For this step, a particular porosity was used to determine the threshold value, and then the resulting depth-averaged 2-D field was used to compute the permeability. After a few iterations, we were able to select the final thresholding value with a consistent effective permeability. In this particular dataset with relatively shallow depth and fractures, the difference of both porosity and permeability values between the depth-averaged 2-D and the original 3-D images was less than 5% and 10% (at a relative scale), respectively. As shown in Figure 1d, the actual porous media is highly non-uniform, exhibiting a wide range of local permeability. Notably, the underground reservoir contains a large number of non-permeable dead-end regions (red arrows), which is often neglected in oil recovery studies.[22,23]

We used this reconstructed 2-D image as a mask for fabricating the model microfluidic reservoir, which is shown in Figure 1e. The device was upscaled to meet the microfabrication limits where the mean permeability is 4.8 μm^2. The microfluidic channels were made *via* standard soft lithography. Polydimethylsiloxane (PDMS; Dow Corning) was poured onto the master mold and cured at 75 °C. Then, the channel was plasma-treated to activate the surface for PVA coating and bonding. A 1 wt % polyvinyl alcohol (PVA) solution was flown through the pre-bonded channel for 10 min. Then, the channel was dried in the oven for complete bonding of the device.

2.2. Pore Flow Simulations. The fluid velocities in this study are small so that the Stokes equation can be used to obtain the velocity field at the pore scale. In this work, the lattice Boltzmann (LB) method was used to solve the steady-state, incompressible water flow using Palabos,[26] an open-source parallel LB solver that has been applied to flow and transport problems in microfluidic devices.[27−30] A 3-D, 19 velocity (D3Q19) model with a single relaxation time in a regular voxel was used with no-slip boundary conditions imposed at all solid boundaries in the micromodel *via* a bounce-back boundary condition. Fixed pressure and normal outflow boundary conditions are imposed along the inlet and outlet, respectively, and the resulting steady flow field is scaled to the Darcy velocity used in the experiment. The model domain was the same as the actual microfluidic device with dimensions of 20 × 2.65 × 0.04 mm^3. A voxel size of 3.1 μm was used. One of the advantages of the LB method is its ability to represent complex pore geometries based on image analysis techniques without the need for further rendering or complex meshing processes. Simple bounce-back boundary conditions can be easily imposed on solid boundaries obtained from the segmented imaging results (Figure 1d), and the resulting flow field is shown in Figure 1f.

2.3. Emulsion Preparation and Interfacial Tension Measurements. Decane emulsion was prepared by adding 10 vol % of decane in water that contains 0.01 M SDS and varying amounts of NaCl. All the chemicals were purchased from Sigma-Aldrich. Then, decane was emulsified using a sonicator and vortex mixer. Decane−water interfacial tension was measured using an inverted pendant drop method. A small volume of decane was pushed into a pool of water from underneath through a syringe needle. An image of the drop attached to the tip of the needle was taken using a camera (Nikon

https://dx.doi.org/10.1021/acs.energyfuels.0c04320
Energy Fuels 2021, 35, 4885−4892

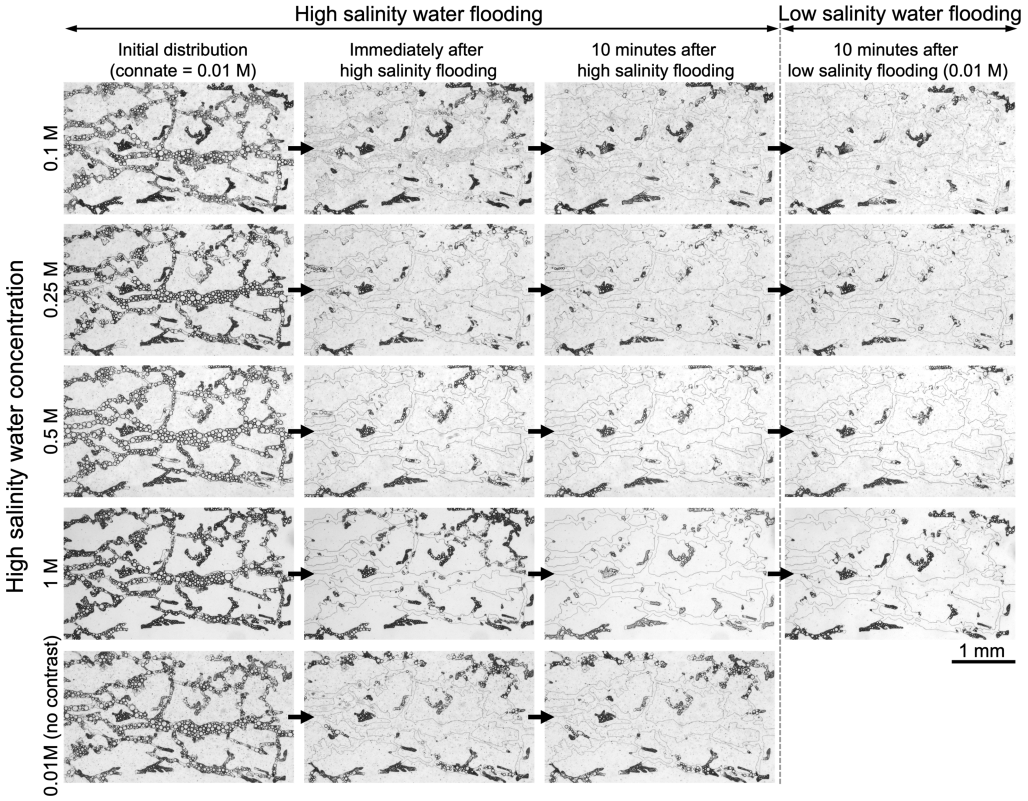

Figure 2. Oil removal in microfluidic porous media by a series of high and low salinity water flooding. Initially, the porous media is filled with decane emulsion containing a 0.01 M NaCl solution (first column). High salinity water is flooded (flow approaching from left to right) where the second column images show immediately upon flooding (~10 s after flooding) and the third column images show 10 min after the flooding. Then, low salinity water (0.01 M NaCl) is injected to mimic low salinity water flooding. All the solutions contain 0.01 M sodium dodecyl sulfate (SDS) for drop stabilization.

D3400) and then processed with MATLAB to obtain the drop curvature and the interfacial tension.

2.4. Microfluidic Experiments and Data Processing. Decane emulsion was filled into an empty channel followed by injection of saline water that also contains 10 mM SDS and varying amounts of NaCl using a syringe pump (Pump 11 Pico Plus Elite, Harvard Apparatus). The drops were visualized with an inverted microscope (DMi8, Leica). The images were processed with ImageJ and MATLAB to obtain the area fraction of the decane emulsion to estimate the recovery factor. To accurately measure the area fraction of the oil drop, the following steps were implemented. Initially, a stack of the bright-field images was imported into ImageJ to remove the background noise by adjusting the image threshold. The boundaries of the oil drops were identified and then filled in with ImageJ. The pore walls were accounted for by processing a blank channel without the oil drops. After binarizing, the images were further processed through MATLAB to count the total pixel intensity, which represents the total oil fraction.

3. RESULTS AND DISCUSSION

3.1. Microfluidic Investigation of Salinity Water Flooding in Model Porous Reservoirs. Using the microfluidic device shown in Figure 1e, we study secondary and tertiary oil recovery with high and low salinity water. The flooding sequence is shown in Figure 2, which mimics high salinity water flooding (secondary recovery) followed by low salinity water flooding (tertiary recovery). We start off by filling the entire porous media with decane emulsion (volume fraction ≈0.1) suspended in 0.01 M NaCl, where the salinity resembles that of relatively fresh groundwater (Figure 2; first column).[31] The size of the oil drops is widely dispersed, ranging from a few microns to nearly 50 μm in diameter. The oil drops are stabilized by adding 0.01 M sodium dodecyl sulfate (SDS) to the suspension, which is one of the most widely used anionic surfactants in enhanced oil recovery.[32] As we aim to focus on the transport aspect of the dynamics of suspended oil drops, we deliberately avoid adhesion and wetting of decane drops on the pore surface by coating the entire channel with PVA, which is a hydrophilic polymer.[33]

Then, we flood the oil-filled porous media with high salinity water (secondary oil recovery; second column in Figure 2). We vary the NaCl concentration of the injecting solution, ranging from 0.01 M (no contrast; control) to 1 M (seawater). The injecting solution also contains 0.01 M SDS to maintain the surfactant concentration constant throughout the experiments so as to mitigate any unwanted surfactant-gradient-induced dynamics. The injection flow rate is kept constant, where the inlet and permeability Reynolds numbers are estimated as, respectively, $\mathrm{Re}_i = \bar{U}_i L/\nu = 0.45$ and $\mathrm{Re}_\kappa = \bar{U}_\kappa \kappa^{1/2}/\nu = 0.0048$, where $\bar{U}_i = 6.9$ mm/s is the inlet mean flow speed, $L = 57$ μm is the hydraulic diameter of the channel inlet, $\bar{U}_\kappa = 2.0$ mm/s is the mean flow speed in the microfluidic porous media, $\kappa = 4.8$ μm^2 is the mean permeability of the porous media, and $\nu = 0.9$ mm^2/s is the kinematic viscosity of the fluid. $\bar{U}_\kappa$ and κ are obtained from numerical simulations (*e.g.*, Figure 1f).

After injecting the high salinity water for 10 min, we switch the injecting solution to 0.01 M NaCl to mimic low salinity water flooding through a high salinity reservoir. The flooding is continued for another 10 min. For each process, we compare before and after images of the porous media, i.e., successive

https://dx.doi.org/10.1021/acs.energyfuels.0c04320
Energy Fuels 2021, 35, 4885−4892

image columns in Figure 2, to estimate the recovered oil drops during a particular experiment. We define the recovery factor as $(n_i - n_f)/n_i$, where n_i and n_f are the area fraction of the oil drops before and after each step, respectively.

Upon initial injection, most of the drops are swept away by the pore flow within 10 s as the drops are freely suspended. However, a substantial amount of oil drops still remain in the dead-end regions due to the lesser influence of the flow, as shown in the second column of Figure 2. The flow simulation results shown in Figure 1f also confirm negligible advection in the dead-end pores. Based on the image analysis, we estimate that roughly 30−40% of the oil drops remain in the pores soon after the injection has taken place (Figure 3a), which happens

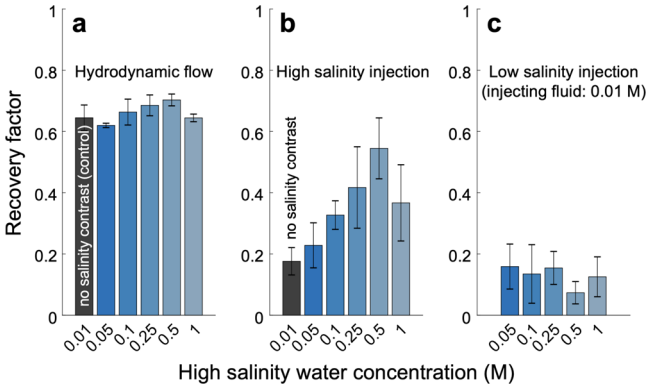

Figure 3. Recovery factors for successive flooding steps. The recovery factors are evaluated and averaged from four different locations including the area shown in Figure 2. (a) Recovery factor immediately after the initial flooding has begun. (b) Recovery factor after 10 min of high salinity water injection. (c) Recovery factor after 10 min of low salinity water injection. The error bars represent standard deviation of results obtained from eight experimental trials across four different pore geometries.

to coincide with the typical recovery efficacy of seawater flooding.[2] The remaining oil drops are more or less constant across various injecting solution salinity (Figure 3a) since the oil transport is mainly governed by hydrodynamics during this stage.

However, after injecting for 10 min and measuring the remaining oil, we observe a stark difference in the recovery factor depending on the salinity of the injecting water; the recovery factor increases with the salt concentration up to 0.5 M followed by a sudden drop at 1 M (Figure 3b). As the saltwater replaces the initially occupying solution, transient salinity gradients are established in the regions in which the fluid flow is negligible compared to diffusion. Such low Péclet number environments easily arise in low- and non-permeable regions such as dead-end pores, as evidenced by the wide distribution of zero velocity regions in the flow field simulations (red arrows in Figure 1f). The salinity gradients that are established within these regions may provide enhanced transport pathways for oil drops *via* non-equilibrium processes, possibly *via* diffusiophoresis and Marangoni propulsion.[34]

Diffusiophoresis is a process by which colloids can spontaneously undergo a directed motion *via* non-equilibrium colloid-solute interactions in the presence of local chemical gradients, where the colloid migration velocity can be expressed as $\mathbf{u} = \mathcal{M}_d \nabla \ln c$.[35] $\mathcal{M}_d$ is the diffusiophoretic mobility that sets the direction and the magnitude of the colloid velocity under a given chemical concentration profile. For negatively charged drops in NaCl solution, as is the case in our experiments since the drops are stabilized with anionic surfactants, $\mathcal{M}_d$ is positive, thus making them migrate up the NaCl concentration gradients;[18] this will cause the drops to migrate out of the dead-ends. Similarly, Marangoni (solutal capillary) propulsion, which arises in the presence of interfacial tension gradients, causes the drops to migrate in the same direction since NaCl reduces the interfacial tension *via* charge screening of the surfactant head groups.[36] Therefore, increasing the salinity contrast will provide more driving force for the drops to escape from the dead-ends *via* the gradient-driven processes, which can contribute to the enhanced recovery factor.

Such a directed motion also implies that a subsequent injection of low salinity water will change the drop motion in the opposite direction, i.e., into the dead-end pore, due to the reversed gradients; this will act against recovering oil. In fact, as shown in Figure 3c the introduction of low salinity water does not provide any substantial improvement in oil recovery. These observations suggest that diffusiophoresis and Marangoni propulsion may not play a favorable role in the oil recovery during low salinity water flooding, but rather beneficial during high salinity water flooding.

3.2. Salinity-Induced Oil Dynamics at High Salinity.

While the gradual enhancement in the recovery factor during high salinity water flooding can be explained by diffusiophoresis and Marangoni effects, it remains unclear why the recovery factor suddenly drops above 0.5 M of the injecting solution (Figure 3b). As we speculate that the variation in the recovery factor is attributed to the oil dynamics occurring in the dead-end pores, we employ idealized dead-end pores to mimic deep dead-ends in the reservoir, which will allow us to better visualize and understand the observed oil recovery trends, particularly at high salinity. A long, slender dead-end pore (width × height × length = 45 × 40 × 800 μm^3) is connected perpendicular to the flow channel (see Figure 4a for example). Experiments are performed similarly to the porous media experiments: (1) fill oil suspension in the dead-end pores; (2) inject high salinity water through the flow channel for 10 min (high salinity water flooding), which will introduce salinity gradients along the pore; and then (3) inject low salinity water (0.01 M) for another 10 min (low salinity water flooding), which will reverse the direction of the salinity gradients within the pore. As the diffusiophoretic motion is induced by the diffusion of solutes, 10 min provides sufficient time scale for the solutes to diffuse across the pore as the salt diffusion time is about $\sim l^2/D = 7$ min, which also corresponds to the characteristic time scale for the duration of diffusiophoresis. Here, $l = 800$ μm is the channel length and $D = 1607$ $\mu m^2/s$ is the ambipolar diffusivity of NaCl in water.[37] The detailed experimental procedure can also be found in our previous diffusiophoresis studies.[38−40]

Figure 4a−c (Movie S1) show the image sequence of drop motion in the straight dead-end pores under various salinity contrasts. At NaCl concentrations below 0.5 M, it is shown that, during the high salinity water flooding (first 10 min), the trapped oil drops gradually migrate toward the pore entrance. Despite the fact that the drops are relatively large and closely packed such that one might expect significant hydrodynamic boundary effects, gradient-induced migration provides sufficient driving force for the drops to migrate persistently along the narrow pores. The main reason for such effective migration

https://dx.doi.org/10.1021/acs.energyfuels.0c04320
Energy Fuels 2021, 35, 4885−4892

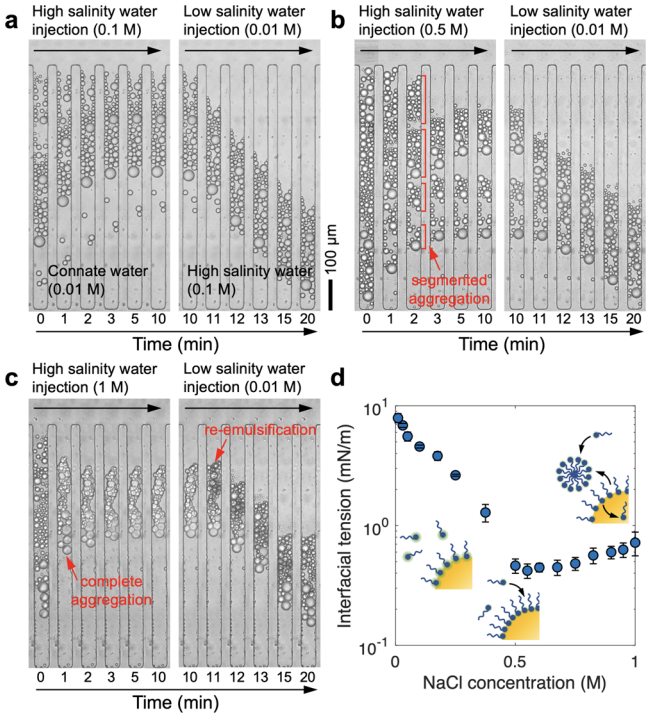

Figure 4. Migration of decane drops in straight dead-end pores by salinity gradients. Similar to porous media experiments shown in Figure 2, we inject high salinity water through a flow channel that is initially filled with decane emulsion suspended in 0.01 M NaCl. After 10 min of injection, we switch to low salinity water injection. We vary the NaCl concentration of injecting solution during high salinity water flooding, where (a) is 0.1 M, (b) is 0.5 M, and (c) is 1 M. All the solutions contain 0.01 M SDS for drop stabilization. (d) Interfacial tension of decane in water with varying NaCl concentrations measured by the reverse pendant drop method. The saline solution also contains 0.01 M SDS. The insets illustrate salinity-dependent surfactant adsorption and desorption at the oil–water interface.

is due to the reduced hydrodynamic interaction experienced by a phoretic particle, where the adjacent flow field induced by the phoretic particle decays much faster ($\sim 1/r^3$) than a particle being dragged through the solution ($\sim 1/r$) such that the phoretic motion is less sensitive to the surroundings. Thus, the drops experience only short-range hydrodynamic interactions with neighboring boundaries,[34] allowing them to slip through the tight pores without experiencing significant hydrodynamic retardation.

The gradient-induced motion gradually slows down over time as the salinity gradient ceases out, which sets the migration distance, and thus the recovery limit. Then, upon low salinity water injection (t>10 min), the drops start to move back into the pore as expected. The asymmetric migration behavior in which the drop migrating into the pore (10<t<20 min) is more persistent than moving out of the pore (0<t<10 min) is attributed to the logarithmic dependence of diffusiophoresis (migration velocity $\mathbf{u} \approx \nabla \ln c$),[17,41] indicating that diffusiophoresis is the dominant migration mechanism over Marangoni propulsion ($\mathbf{u} \approx \nabla c$) presumably due to the large zeta potential of the surfactant-stabilized drops (≈ -90 mV)[38] and small interfacial tension difference induced by NaCl gradients.[18]

The gradient-dependent directional migration is consistent up to 0.5 M. However, at 1 M, we observe a peculiar behavior in which the drops start to rapidly adhere to one another soon after being exposed to the high salinity water (Figure 4c). Such a rapid aggregation results in the formation of a large oil cluster, which grows large enough to subsequently block the pore so that it stops moving immediately (~2 min). The blockage is not a consequence of drops wetting on the wall, but by continuous aggregation of freely suspended drops.

The rapid demulsification appears to be attributed to the reduced electrostatic repulsion between the drops, thus allowing the drops to approach closer and subsequently adhere together by the attractive van der Waals interaction. However, due to the surfactants present at the interface, the drops do not completely coalesce, but they undergo a partial coalescence, resulting in a foam-like structure (Figure 4c). The formation of such structures depends on the stability of the thin film present in between the adjoining drops, which is determined by the electrostatic, van der Waals, and steric interactions that set the disjoining pressure of the film.[42]

Another unconventional mechanism that can possibly contribute to the partial coalescence is the salting-out effect.[43] Due to the excess amount of NaCl present in high salinity water, the surfactants can be "salted out" from the interface, resulting in increased interfacial tension. For instance, Figure 4d shows the salinity-dependent decane–water interfacial tension measured by the reverse pendant drop method. As commonly expected, the interfacial tension decreases as the NaCl concentration is increased until 0.5 M due to the charge screening.[36] However, the trend reverses more or less above 0.5 M where the interfacial tension starts to increase with NaCl concentration, which is the direct evidence of the salting-out effect. The salted-out surfactants can then form micro-emulsion,[43] micelles,[44] or aggregates,[45] all of which can contribute to the increased stability of the thin film present between the drops and thus the partial coalescence.

The salinity-induced rapid demulsification acts against oil recovery, which is the key reason for the reduced recovery factor at high salinity (1 M) in the porous media experiments. The dead-ends found in the actual subsurface are seldom straight, but rather curved or branched with a narrow neck, as shown in Figure 1. These features make the aggregated oil clusters to be tightly locked in place, making them even harder to recover (Figure 5a). As we estimate the recovery factor in dead-end pores for various injection concentrations, we observe a similar trend as in porous media, where the recovery factor gradually increases up to 0.5 M followed by a sudden drop at 1 M, as shown in Figure 5b. We note that the reverse diffusioosmotic flow occurring along the pore surface does not play a role in the oil dynamics due to the presence of PVA coating on the pore walls, which is often used in PDMS-based microfluidic devices to minimize any electrokinetic phenomena.[46]

3.3. Enhanced Drop Removal at Intermediate Salinity by Partial Clustering. The consequence of drop aggregation is not always detrimental to the oil recovery, but it also offers some promising aspects. As the electrostatic and salting-out effects depend on the salinity, the degree to which the partial coalescence occurs is observed to be dependent on the salt concentration. For instance, while the NaCl concentration at 0.1 M shows no visible drop–drop adhesion, as observed from the intact spherical boundaries of the drops shown in the top panel of Figure 6a, at 0.5 M, we start to observe a weak drop adhesion as evidenced by the distinct contact interfaces (Figure 6a, middle panel). At 1 M, we observe a strong demulsification, which is characterized by more aggressive

https://dx.doi.org/10.1021/acs.energyfuels.0c04320
Energy Fuels 2021, 35, 4885–4892

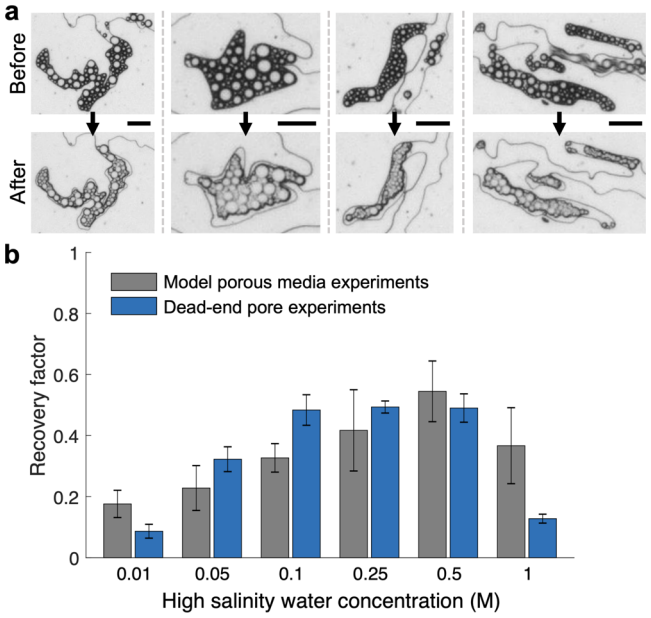

Figure 5. Salinity-induced drop aggregation hinders oil recovery. (a) Some close-up images of oil demulsification in deep dead-ends in the porous media experiments during high salinity water flooding (1 M NaCl). Images in the top and bottom rows are taken, respectively, before and after flooding the porous media with 1 M NaCl for 10 min. All the scale bars are 100 μm. (b) Recovery factors obtained from the dead-end pore experiments in Figure 4 during high salinity water flooding (blue bars). For comparison, similar data for porous media experiments under similar experimental conditions (Figure 3b) are also included (gray bars). The error bars for the dead-end pore experiments represent the standard deviation of four experimental runs, where each run is an average of five measurements from the five neighboring pores.

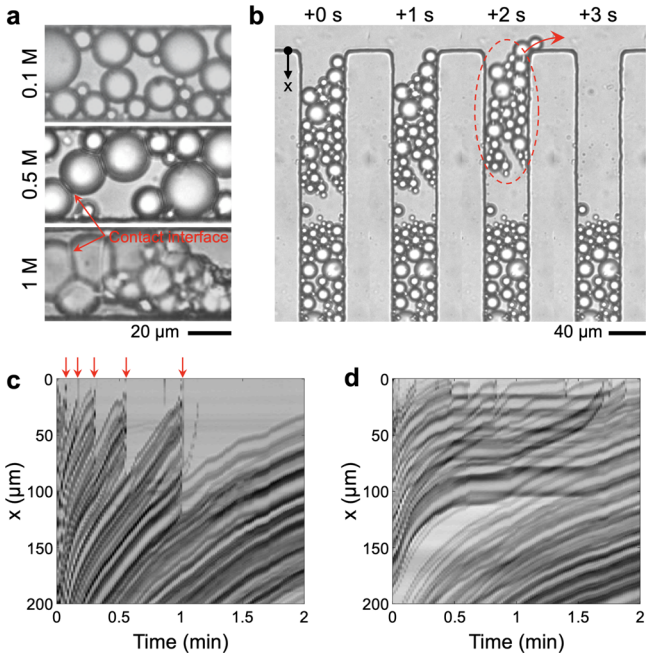

Figure 6. Weak drop adhesion allows enhanced drop recovery from the dead-end pores. (a) Close-up images of decane drops suspended at different salinity water 10 min after high salinity water flooding. Images at 0.5 and 1 M show visible partial coalescence. (b) Image sequence of clustered drops escaping during high salinity water flooding with 0.5 M NaCl. (c, d) Kymographs of the decane drops during high salinity water flooding with (c) 0.5 M NaCl and (d) 0.1 M NaCl (from Figure 4a,b).

aggregation with a significantly larger contact area due to the reduced electrostatic repulsion and surfactant salting-out effect (Figure 6a, bottom panel).

Interestingly, the ways in which the drops escape from the pores differ depending on the degree of drop−drop adhesion. While the strong drop aggregation at 1 M does not allow the drops to escape (because of the blockage), the drops at 0.5 M are loosely adhered to form smaller segments (*e.g.*, see the transition between 0 and 2 min in Figure 4b) that allows migration toward the pore entrance *via* diffusiophoresis. As the drops approach near the entrance where the channel flow becomes significant ($x \approx$ pore width[47]), the drops begin to experience strong viscous drag from the main channel flow, which carries away the drops. Since the drops are held together, once the leading side of the cluster reaches the pore entrance, the fluid shear drags the cluster so that the entire cluster is pulled out of the pore immediately (Figure 6b).

Such an effective oil removal is clearly captured in the kymograph of the drops analyzed from the results in Figure 4b (or Figure 6b), as shown in Figure 6c. The dark streaks represent the drop trajectories. It is shown that the adhesion-mediated removal is observed by the sudden disappearance of the drop trajectories. The effect continues until the salinity gradients cease out, as indicated by the red arrows in Figure 6c. The consequence of such clustered oil removal is the enhanced recovery efficiency. On the other hand, at 0.1 M where no aggregation is observed, the drops escape from the pore individually one by one (Figure 6d). Such salinity-dependent oil dynamics indicate that an optimal operation condition may exist for high salinity water flooding, suggesting a potential strategy to maximize oil recovery.

It is noteworthy to mention that the rapid demulsification is not irreversible as they can be re-emulsified when exposed to low salinity water. During the subsequent low salinity water injection, the cluster starts to re-emulsify as shown in the latter stage (t>10 min) in Figure 4c. Subsequently, the released individual drops are able to undergo diffusiophoresis once again, which now makes the drops to go even further deep into the pore, thus hindering the oil recovery process.

4. CONCLUSIONS

In summary, we have demonstrated how salinity-dependent drop−drop and drop−solute interactions can directly impact the local oil dynamics in porous media and thus the recovery performance during high and low salinity flooding. Using full 3-D, actual subsurface data, we have created a 2-D microfluidic reservoir for studying oil recovery on a miniaturized chip. By injecting high and low salinity water to the microfluidic porous media, which mimics, respectively, the secondary and tertiary recovery processes, we have shown that the oil recovery can be significantly influenced by the salinity of the injected solution. Our results reveal that the oil recovery enhances as the salinity is increased in high salinity water flooding due to the gradient-driven transport processes taking place in the deep pore space. However, above a critical salinity, which we found to be ∼0.5 M in our experiments, we observed a rapid aggregation of drops that led to the complete blockage of the pore, thereby hindering oil recovery. We have also found that, at intermediate salinity where the drop aggregation is mild, the

https://dx.doi.org/10.1021/acs.energyfuels.0c04320
Energy Fuels 2021, 35, 4885−4892

drop aggregation, in combination with diffusiophoresis, in fact helps oil recovery. Moreover, as we have recently identified that suspended colloids can be trapped and rapidly grow into a large cluster near merging flow junctions *via* diffusiophoresis,[48−50] the salinity-induced drop aggregation may possibly arise not only in impervious dead-ends but also in permeable pore networks, suggesting that the gradient-driven transport processes may be prevalent across the entire porous media during flooding during certain operating conditions. Our study also warrants a combined study of oil and fines transport and wetting phenomena induced by the salinity change to gain a holistic understanding of the high and low-salinity water flooding processes.[51]

■ ASSOCIATED CONTENT

Supporting Information

The Supporting Information is available free of charge at https://pubs.acs.org/doi/10.1021/acs.energyfuels.0c04320.

(Movie S1) Migration of decane drops in dead-end pores upon high and low salinity water injection (play speed is 30×) (AVI)

■ AUTHOR INFORMATION

Corresponding Author

Sangwoo Shin − *Department of Mechanical Engineering, University of Hawaii at Manoa, Honolulu, Hawaii 96822, United States;* orcid.org/0000-0001-5618-8522; Email: sangwoos@hawaii.edu

Authors

Sung wan Park − *Department of Mechanical Engineering, University of Hawaii at Manoa, Honolulu, Hawaii 96822, United States*

Jonghyun Lee − *Department of Civil and Environmental Engineering & Water Resources Research Center, University of Hawaii at Manoa, Honolulu, Hawaii 96822, United States*

Hongkyu Yoon − *Geomechanics Department, Sandia National Laboratories, Albuquerque, New Mexico 87123, United States;* orcid.org/0000-0001-6719-280X

Complete contact information is available at: https://pubs.acs.org/10.1021/acs.energyfuels.0c04320

Notes

The authors declare no competing financial interest.

■ ACKNOWLEDGMENTS

This material is based upon work supported by the National Science Foundation under grant no. CBET-1930691. Sandia National Laboratories is a multimission laboratory managed and operated by National Technology and Engineering Solutions of Sandia, LLC, a wholly owned subsidiary of Honeywell International, Inc., for the U.S. Department of Energy's National Nuclear Security Administration under contract DE-NA-0003525. This paper describes objective technical results and analysis. Any subjective views or opinions that might be expressed in the paper do not necessarily represent the views of the U.S. Department of Energy or the United States Government.

■ REFERENCES

(1) Looney, B. *Statistical Review of World Energy 2020, 69th Edition*; bp 2020.

(2) Muggeridge, A.; Cockin, A.; Webb, K.; Frampton, H.; Collins, I.; Moulds, T.; Salino, P. Recovery rates, enhanced oil recovery and technological limits. *Philos. Trans. R. Soc. A* **2014**, *372*, 20120320.

(3) Seyyedi, M.; Tagliaferri, S.; Abatzis, J.; Nielsen, S. M. An integrated experimental approach to quantify the oil recovery potential of seawater and low-salinity seawater injection in North Sea chalk oil reservoirs. *Fuel* **2018**, *232*, 267−278.

(4) Sheng, J. J. *Modern Chemical Enhanced Oil Recovery: Theory and Practice*; Gulf Professional Publishing, 2011.

(5) Morrow, N. R.; Tang, G.-q.; Valat, M.; Xie, X. Prospects of improved oil recovery related to wettability and brine composition. *J. Pet. Sci. Eng.* **1998**, *20*, 267−276.

(6) Nasralla, R. A.; Nasr-El-Din, H. A. Double-layer expansion: is it a primary mechanism of improved oil recovery by low-salinity waterflooding? *SPE Reserv. Eval. Eng.* **2014**, *17*, 49−59.

(7) Sheng, J. J. Critical review of low-salinity waterflooding. *J. Pet. Sci. Eng.* **2014**, *120*, 216−224.

(8) Katende, A.; Sagala, F. A critical review of low salinity water flooding: Mechanism, laboratory and field application. *J. Mol. Liq.* **2019**, *278*, 627−649.

(9) Kakati, A.; Kumar, G.; Sangwai, J. S. Oil recovery efficiency and mechanism of low salinity-enhanced oil recovery for light crude oil with a low acid number. *ACS Omega* **2020**, *5*, 1506−1518.

(10) Hua, Z.; Li, M.; Ni, X.; Wang, H.; Yang, Z.; Lin, M. Effect of injection brine composition on wettability and oil recovery in sandstone reservoirs. *Fuel* **2016**, *182*, 687−695.

(11) Jha, R. K.; John, A. K.; Bryant, S. L.; Lake, L. W. Flow reversal and mixing. *SPE J.* **2009**, *14*, 41−49.

(12) Homsy, G. M. Viscous fingering in porous media. *Annu. Rev. Fluid Mech.* **1987**, *19*, 271−311.

(13) Kar, A.; Chiang, T.-Y.; Rivera, I. O.; Sen, A.; Velegol, D. Enhanced transport into and out of dead-end pores. *ACS Nano* **2015**, *9*, 746−753.

(14) Shin, S.; Um, E.; Sabass, B.; Ault, J. T.; Rahimi, M.; Warren, P. B.; Stone, H. A. Size-dependent control of colloid transport via solute gradients in dead-end channels. *Proc. Natl. Acad. Sci. U. S. A.* **2016**, *113*, 257−261.

(15) Velegol, D.; Garg, A.; Guha, R.; Kar, A.; Kumar, M. Origins of concentration gradients for diffusiophoresis. *Soft Matter* **2016**, *12*, 4686−4703.

(16) Ault, J. T.; Warren, P. B.; Shin, S.; Stone, H. A. Diffusiophoresis in one-dimensional solute gradients. *Soft Matter* **2017**, *13*, 9015−9023.

(17) Shin, S.; Warren, P. B.; Stone, H. A. Cleaning by Surfactant Gradients: Particulate Removal from Porous Materials and the Significance of Rinsing in Laundry Detergency. *Phys. Rev. Appl.* **2018**, *9*, No. 034012.

(18) Yang, F.; Shin, S.; Stone, H. A. Diffusiophoresis of a charged drop. *J. Fluid Mech.* **2018**, *852*, 37−59.

(19) Mashat, A.; Shi, N.; Squires, T.; Abdel-Fattah, A. Autonomous Reservoir Nano-Agents. *SPE Middle East Oil and Gas Show and Conference*; Society of Petroleum Engineers 2019.

(20) Shi, N.; Mashat, A.; Abdel-Fattah, A. Autonomous Nano-Surfactant for Enhanced Oil Recovery Applications. *SPE Europec featured at 82nd EAGE Conference and Exhibition*; Society of Petroleum Engineers 2020.

(21) Howe, A. M.; Clarke, A.; Mitchell, J.; Staniland, J.; Hawkes, L.; Whalan, C. Visualising surfactant enhanced oil recovery. *Colloids Surf., A* **2015**, *480*, 449−461.

(22) Xu, K.; Agrawal, D.; Darugar, Q. Hydrophilic nanoparticle-based enhanced oil recovery: microfluidic investigations on mechanisms. *Energy Fuels* **2018**, *32*, 11243−11252.

(23) Lifton, V. A. Microfluidics: an enabling screening technology for enhanced oil recovery (EOR). *Lab Chip* **2016**, *16*, 1777−1796.

(24) Petrusak, R.; Jason, H.; Dewers, T.; Goad, P.; Esposito, R. *Characteristics of seal formations (confining units) for CO2 injection in*

the Lower Tuscaloosa Sandstones in Southeastern Mississippi; The Eighth Annual Conference on Carbon Capture & Sequestration: Pittsburgh, PA. 2009.
(25) Yoon, H.; Dewers, T. A. Nanopore structures, statistically representative elementary volumes, and transport properties of chalk. *Geophys. Res. Lett.* **2013**, *40*, 4294−4298.
(26) Latt, J.; Malaspinas, O.; Kontaxakis, D.; Parmigiani, A.; Lagrava, D.; Brogi, F.; Belgacem, M. B.; Thorimbert, Y.; Leclaire, S.; Li, S.; Marson, F.; Lemus, J.; Kotsalos, C.; Conradin, R.; Coreixas, C.; Petkantchin, R.; Raynaud, F.; Beny, J.; Chopard, B. Palabos: Parallel Lattice Boltzmann Solver. *Comput. Math. Appl.* **2021**, *81*, 334−350.
(27) Yoon, H.; Valocchi, A. J.; Werth, C. J.; Dewers, T. Pore-scale simulation of mixing-induced calcium carbonate precipitation and dissolution in a microfluidic pore network. *Water Resour. Res.* **2012**, *48*, W02524.
(28) Yoon, H.; Kang, Q.; Valocchi, A. J. Lattice Boltzmann-Based Approaches for Pore-Scale Reactive Transport. *Rev. Mineral. Geochem.* **2015**, *80*, 393−431.
(29) Yoon, H.; Chojnicki, K. N.; Martinez, M. J. Pore-Scale Analysis of Calcium Carbonate Precipitation and Dissolution Kinetics in a Microfluidic Device. *Environ. Sci. Technol.* **2019**, *53*, 14233−14242.
(30) Boyd, B.; Yoon, H.; Zhang, C.; Oostrom, M.; Hess, N.; Fouke, B.; Valocchi, A. J.; Werth, C. J. Influence of Mg^{2+} on $CaCO_3$ precipitation during subsurface reactive transport in a homogeneous silicon-etched pore network. *Geochim. Cosmochim. Acta* **2014**, *135*, 321−335.
(31) akeman, A. J.; Barreteau, O.; Hunt, R. J.; Rinaudo, J.-D.; Ross, A. *Integrated Groundwater Management*; Springer Nature, 2016.
(32) Negin, C.; Ali, S.; Xie, Q. Most common surfactants employed in chemical enhanced oil recovery. *Petroleum* **2017**, *3*, 197−211.
(33) Trantidou, T.; Elani, Y.; Parsons, E.; Ces, O. Hydrophilic surface modification of PDMS for droplet microfluidics using a simple, quick, and robust method via PVA deposition. *Microsyst. Nanoeng.* **2017**, *3*, 16091.
(34) Anderson, J. L. Colloid transport by interfacial forces. *Annu. Rev. Fluid Mech.* **1989**, *21*, 61−99.
(35) Shin, S. Diffusiophoretic separation of colloids in microfluidic flows. *Phys. Fluids* **2020**, *32*, 101302.
(36) Beunen, J. A.; Ruckenstein, E. The effect of salting out and micellization on interfacial tension. *Adv. Colloid Interface Sci.* **1982**, *16*, 201−231.
(37) Cussler, E. L. *Diffusion: Mass Transfer in Fluid Systems*, 3rd ed.; Cambridge University Press: Cambridge, UK, 2009.
(38) Shin, S.; Ault, J. T.; Feng, J.; Warren, P. B.; Stone, H. A. Low-cost zeta potentiometry using solute gradients. *Adv. Mater.* **2017**, *29*, 1701516.
(39) Shin, S.; Doan, V. S.; Feng, J. Osmotic delivery and release of lipid-encapsulated molecules via sequential solution exchange. *Phys. Rev. Appl.* **2019**, *12*, No. 024014.
(40) Doan, V. S.; Saingam, P.; Yan, T.; Shin, S. A trace amount of surfactants enables diffusiophoretic swimming of bacteria. *ACS Nano* **2020**, *14*, 14219−14227.
(41) Palacci, J.; Abécassis, B.; Cottin-Bizonne, C.; Ybert, C.; Bocquet, L. Colloidal motility and pattern formation under rectified diffusiophoresis. *Phys. Rev. Lett.* **2010**, *104*, 138302.
(42) Stubenrauch, C.; von Klitzing, R. Disjoining pressure in thin liquid foam and emulsion films−new concepts and perspectives. *J. Phys. Condens. Matter* **2003**, *15*, R1197.
(43) Ruckenstein, E.; Krishnan, R. Effect of electrolytes and mixtures of surfactants on the oil-water interfacial tension and their role in formation of microemulsions. *J. Colloid Interface Sci.* **1980**, *76*, 201−211.
(44) Wang, S.; Chen, C.; Kadum, M. J.; Shiau, B.-J.; Harwell, J. H. Enhancing foam stability in porous media by applying nanoparticles. *J. Dispersion Sci. Technol.* **2018**, *39*, 734−743.
(45) Xu, H.-N.; Liu, Y.; Zhang, L. Salting-out and salting-in: competitive effects of salt on the aggregation behavior of soy protein particles and their emulsifying properties. *Soft Matter* **2015**, *11*, 5926−5932.
(46) Kaniansky, D.; Masár, M.; Bielčíková, J. Electroosmotic flow suppressing additives for capillary zone electrophoresis in a hydrodynamically closed separation system. *J. Chromatogr. A* **1997**, *792*, 483−494.
(47) Battat, S.; Ault, J. T.; Shin, S.; Khodaparast, S.; Stone, H. A. Particle entrainment in dead-end pores by diffusiophoresis. *Soft Matter* **2019**, *15*, 3879−3885.
(48) Shin, S.; Ault, J. T.; Warren, P. B.; Stone, H. A. Accumulation of colloidal particles in flow junctions induced by fluid flow and diffusiophoresis. *Phys. Rev. X* **2017**, *7*, No. 041038.
(49) Ault, J. T.; Shin, S.; Stone, H. A. Diffusiophoresis in narrow channel flows. *J. Fluid Mech.* **2018**, *854*, 420−448.
(50) Shin, S.; Ault, J. T.; Toda-Peters, K.; Shen, A. Q. Particle trapping in merging flow junctions by fluid-solute-colloid-boundary interactions. *Phys. Rev. Fluids* **2020**, *5*, No. 024304.
(51) Liu, F.; Wang, M. Review of low salinity waterflooding mechanisms: Wettability alteration and its impact on oil recovery. *Fuel* **2020**, *267*, 117112.

https://dx.doi.org/10.1021/acs.energyfuels.0c04320
Energy Fuels 2021, 35, 4885−4892